Published in final edited form as:
J Nucl Med. 2012 June ; 53(6): 908–916. doi:10.2967/jnumed.111.100545.

In vivo imaging of endogenous pancreatic beta cell mass in healthy and type 1 diabetic subjects using [^{18}F]FP-(+)-DTBZ and PET

Marc D. Normandin[1], **Kitt F. Petersen**[2], **Yu-Shin Ding**[1], **Shu-Fei Lin**[1], **Sarita Naik**[2], **Krista Fowles**[1], **Daniel M. Skovronsky**[3], **Kevan C. Herold**[4], **Timothy J. McCarthy**[5], **Roberto A. Calle**[5], **Richard E. Carson**[1], **Judith L. Treadway**[5], and **Gary W. Cline**[2]

[1]Department of Diagnostic Radiology, Yale University, 801 Howard Avenue, New Haven, CT 06520

[2]Department of Endocrinology, Yale University, 15 York Street, New Haven, CT 06510

[3]Avid Radiopharmaceuticals, 3711 Market Street, Philadelphia, Pennsylvania 19104

[4]Department of Immunobiology, Yale University, 300 Cedar Street, New Haven, CT 06520

[5]Pfizer Global R&D, Eastern Point Road, Groton, CT 06340

Abstract

The ability to non-invasively measure endogenous pancreatic β-cell mass (BCM) would accelerate research on the pathophysiology of diabetes and revolutionize the preclinical development of new treatments, the clinical assessment of therapeutic efficacy, and the early diagnosis and subsequent monitoring of disease progression. The vesicular monoamine transporter type 2 (VMAT2) is co-expressed with insulin in β-cells and represents a promising target for BCM imaging.

Methods—We evaluated the VMAT2 radiotracer ^{18}F-fluoropropyl-dihydrotetrabenazine ([^{18}F]FP-(+)-DTBZ, also known as [^{18}F]AV-133) for quantitative positron emission tomography (PET) imaging of BCM in healthy control subjects and patients with type 1 diabetes mellitus (T1DM). Standardized uptake value (SUV) was calculated as the net tracer uptake in pancreas normalized by injected dose and body weight. Total volume of distribution *(V_T)*, the equilibrium ratio of tracer concentration in tissue relative to plasma, was estimated by kinetic modeling with arterial input functions. Binding potential *(BP_{ND})*, the steady-state ratio of specific binding to non-displaceable uptake, was calculated using the renal cortex as a reference tissue devoid of specific VMAT2 binding.

Results—Mean pancreatic SUV, V_T, and BP_{ND} were reduced by 38%, 20% and 40%, respectively, in T1DM. The radiotracer binding parameters correlated with insulin secretion capacity as determined by arginine-stimulus tests. Group differences and correlations with β-cell function were enhanced for total pancreas binding parameters that accounted for tracer binding density as well as organ volume.

Conclusion—These findings demonstrate that quantitative evaluation of islet β-cell density and aggregate BCM can be performed clinically with [^{18}F]FP-(+)-DTBZ PET.

Corresponding author address: Gary W. Cline, Yale University School of Medicine, Department of Endocrinology, P.O. Box 208020, New Haven, CT 06520, 203-785-5934, gary.cline@yale.edu. First author address: Marc D. Normandin, Massachusetts General Hospital, Division of Nuclear Medicine and Molecular Imaging, 55 Fruit Street, White 427, Boston, MA 02114, 617-643-6836, normandin@pet.mgh.harvard.edu.

Disclosures: T.J.M., R.A.C., and J.L.T. are employees of Pfizer, which provided funding for the experiments through the Yale-Pfizer Bioimaging Alliance. D.M.S. is an employee Avid Radiopharmaceuticals, which provided the PET radiotracer.

Keywords

Diabetes; pancreas; beta cell mass; PET

The lack of robust methods for non-invasive imaging of endogenous pancreatic islet β-cell mass (BCM) hampers the development of treatments to prevent or reverse the loss of BCM in type 1 diabetes mellitus (T1DM). Strategies for imaging BCM by positron emission tomography (PET) and single photon emission tomography (SPECT) using radiotracers targeted to β-cell-specific binding sites have been explored (1–9). Of the radioligands identified to date, only those targeting vesicular monoamine transporter type 2 (VMAT2) have warranted phase 1 clinical evaluation for quantitative imaging of BCM in humans (5–9).

VMAT2 is responsible for the storage and release of monoamines such as dopamine, norepinephrine, and serotonin in the transport vesicles of synaptic terminals of monoaminergic neurons (10,11). Imaging of VMAT2 alterations in the brain associated with Parkinson's disease have been successfully studied using PET imaging of [^{11}C]dihydrotetrabenazine ([^{11}C]DTBZ) binding to VMAT2 (12,13). VMAT2 has also been found to be co-expressed with insulin in pancreatic β-cells (14–16). Preclinical PET studies in rodents demonstrated diminished pancreatic binding of [^{11}C]DTBZ and its ^{18}F-labeled fluoropropyl derivative, [^{18}F]FP-(+)-DTBZ (also known as [^{18}F]AV-133), in concert with depletion of BCM (7,8,17). A recent PET imaging study in humans showed a correlative reduction in [^{11}C]DTBZ binding in the pancreas in type-1 diabetic (T1DM) patients as compared to healthy controls (9). The modest reduction in pancreatic binding potential in the C-peptide negative T1DM subjects and significant background binding of [^{11}C]DTBZ compromised its efficacy as a diagnostic tool to evaluate the effectiveness of therapies designed to slow or reverse loss of BCM.

The enhanced binding affinity of [^{18}F]FP-(+)-DTBZ at VMAT2 (~8-fold lower Ki compared to [^{11}C]DTBZ) led us to hypothesize that [^{18}F]FP-(+)-DTBZ would exhibit a substantial improvement in its dynamic range for quantitative PET imaging of BCM. Here we combined measurements from [^{18}F]FP-(+)-DTBZ PET and arginine stimulus tests to assess pancreatic BCM *in vivo* and determine its relationship to insulin secretion capacity. Arterial blood data collected during PET imaging were analyzed to determine the time course of the radioligand concentration in plasma for tracer kinetic modeling of regional time activity curves. Analysis with a compartmental model yielded the volume of distribution (V_T), a quantity that reflects the equilibrium concentration of the tracer in tissue relative to the amount available in the plasma. Using V_T in kidney as a measure of non-specific uptake, we calculated binding potential (BP_{ND}), an index of specific binding (18), in total pancreas and the head, body and tail subregions of the organ. The tracer binding parameters V_T and BP_{ND} were found to correlate with insulin secretion capacity as determined from arginine stimulus tests, demonstrating the relationship between [^{18}F]FP-(+)-DTBZ binding in pancreas and β-cell function. Correcting binding parameters by pancreas volume determined by magnetic resonance imaging yielded a measure of total BCM, which exhibited even greater group differences in tracer binding and more pronounced correlation with insulin secretion capacity. Our results indicate that [^{18}F]FP-(+)-DTBZ can clearly discern the loss of BCM in T1DM subjects and is likely to be highly useful for longitudinal studies to evaluate preservation of BCM in diabetic subjects after treatment.

MATERIALS AND METHODS

Subjects

The protocol was approved by the Yale University Human Investigation Committee. Each subject provided written informed consent after the purpose, nature and potential complications of the studies were explained and prior to their participation in the experiments. The studies were conducted according to the principles expressed in the Declaration of Helsinki.

Men and women between the ages of 18 and 55 years of age were recruited from the New Haven community by local advertisement. From this recruitment we sequentially studied 16 subjects. Patients with T1DM as defined by ADA criteria were screened. Enrolled participants had a duration of diabetes of more than 9 years, had a fasting C-peptide 0.1 $ng.mL^{-1}$, and a BMI between 21 and 29 $kg.m^{-2}$. Healthy volunteers matched for age and body mass index with no history of Type 1 diabetes, fasting blood glucose 100 $mg.L^{-1}$, and testing negative for islet autoantibodies were enrolled. Relevant demographics and laboratory results are highlighted in Table 1.

β-Cell Function: Arginine and Glucose-Glucagon Stimulus Tests

β-cell function was determined by measuring the serum C-peptide response following a bolus injection of arginine. All subjects were studied as outpatients after an overnight fast. T1DM subjects were instructed to not take their usual morning insulin dose. Two antecubital venous catheters were inserted, one for arginine injection and the other for collection of fasting blood samples to determine the levels of glucose, C-peptide, and other hormones. A bolus injection of 5 g of 10% arginine-hydrochloride in phosphate-buffered saline was infused over 1 minute. Blood samples were collected at 0, 3, 4, 5, and 6 minutes.

In a select group of subjects (n=4 controls and n=3 T1DM patients), functional beta cell responses were evaluated using a two-phase glucose clamp followed by a glucagon stimulation test, modified from methods by Keymeulen *et al* (19). This methodology was chosen to give maximal -cell stimulation to detect any residual β-cell function in the T1DM subjects that was not identifiable in the acute arginine stimulus test. Glucose levels were maintained between 90 and 100 $mg{\cdot}dL^{-1}$ for the first phase of the clamp (0 – 90 minutes). During the second phase (90 – 210 minutes), glucose levels were increased to 300 $mg{\cdot}dL^{-1}$ as described by De Fronzo *et al* (20) and subsequently maintained between 300 and 350 $mg{\cdot}dL^{-1}$. At 210 minutes, 1mg glucagon was given intravenously. C-peptide measurements were obtained at 0, 150, 180, 210, 212, 213, 214 and 215 minutes.

For both the arginine and glucagon challenge paradigms, plasma glucose concentrations were measured using an YSI STAT 2700 Analyzer (Yellow Springs, CA) and plasma C-peptide samples were analyzed using the Double Antibody immunoassay (Siemens Healthcare Diagnostics, Deerfield, IL).

Magnetic Resonance Imaging

A magnetic resonance image of the trunk was acquired in each subject using a Siemens Sonata 1.5T Instrument (multi-breathhold T1-weighted acquisition, field of view: 38.0 × 38.0 cm, matrix = 256 × 256, in-plane resolution = 1.48 mm, 50 contiguous slices; 5 mm slice thickness). The pancreas was identified interactively using the BioImage Suite software package (21). The segmentation map was summed to determine total volume of the pancreas for each subject.

Radiosynthesis of [^{18}F]FP-(+)-DTBZ

[^{18}F]FP-(+)-DTBZ was obtained from Avid Radiopharmaceuticals (Philadelphia, PA). Specific activity at time of radiotracer injection was 29.2±9.7 MBq·nmol^{-1}.

Positron Emission Tomography Imaging

All subjects were studied after an overnight fast. Type I diabetic subjects were instructed to not take their usual morning insulin dose. A radial arterial catheter was inserted for blood sampling and an antecubital venous catheter was inserted for radiotracer infusion. When warranted, a second venous catheter was placed for the infusion of glucose in the diabetic subjects. Blood glucose was measured at 30 minute intervals and insulin dosage (via injection or insulin pump rate) or glucose infusions were adjusted as needed to maintain euglycemia in the diabetic subjects. Heart rate, blood pressure, and electrocardiogram were monitored continuously throughout the imaging procedure.

Subjects were scanned using an ECAT EXACT HR+ PET camera (CTI/Siemens, Knoxville, Tennessee, United States) with reconstructed spatial resolution of approximately 6 mm (22). Data acquisition occurred over a period of up to 360 minutes with breaks of approximately 30 minutes duration at 120 and 240 minutes. Transmission scans at each of three bed positions were acquired at the beginning of each session. Dynamic PET measurements were acquired in 2D mode, cycling between three sequential bed positions that covered a 420 mm axial field of view over the abdomen. [^{18}F]FP-(+)-DTBZ (348±30 MBq) was administered as a slow bolus over 5 minutes immediately after the start of the scan. There were no differences between control and T1DM subjects in injected radioactivity (342±35 vs. 356±23 MBq, P=0.36) or mass (7.57±3.70 vs. 7.34±1.77 nmol, P=0.88). PET images were reconstructed using an ordered subsets expectation maximization (OSEM; 16 subsets, 2 iterations) algorithm with corrections for scatter, attenuation, scanner dead-time, detector normalization, and radioactive decay. Final images had 2.57 mm isotropic voxels of dimension 256×256×163.

Arterial Input Function Measurement

Arterial cannulation was successfully performed in 6 T1DM patients and 8 healthy controls. For these subjects, radioactivity concentration in arterial blood was measured continuously using an integrated peristaltic pump and calibrated radioactivity detector (PBS101, Veenstra Instruments, Joure, The Netherlands) for the first 10 min after radiotracer administration with 1 discrete sample manually obtained at 7 min. Serial samples were collected manually thereafter with progressively increasing duration between blood draws. Manual samples were measured on a gamma counter to determine radioactivity concentration in whole blood and centrifuged to determine plasma radioactivity concentration. The whole blood-plasma ratio was determined and used to scale the continuous whole blood concentration data measured by the continuous blood counter used at the beginning of the scan.

Arterial samples collected at 7, 12, 20, 30, 45, 60, 90, 120, 180, and 240 minutes post-injection were analyzed for the fraction of unchanged [^{18}F]FP-(+)-DTBZ and its metabolites using a column-switching high performance liquid chromatography assay (23). The supernatant plasma samples were obtained through centrifuging EDTA whole blood samples at 2300g at 4°C for 5 min. Clear plasma mixture with urea at a final concentration of 8M was then filtered through 0.45 μm Millipore Millex-HA syringe filter. Activity in the filtrated plasma sample and the filter were counted with the automatic PerkinElmer gamma well-counter for obtaining sample recovery rate and extraction efficiency. Up to 5 mL of the plasma sample was loaded onto the self-packed capture column with Phenomenex SPE C18 Strata-X sorbent with 1% acetonitrile water at 2 mL·min^{-1}. The analytical mobile phase designated 60: 40 0.1M Ammonium formate: acetonitrile at 1.5 mL·min^{-1} coupled with

Phenomenex Luna C18 analytical column (250×4.6mm, 5μm) gave the FP-(+)-DTBZ parent compound retention time at 10 min. All the HPLC eluent was fraction-collected by an automated Spectrum Chromatography CF-1 fraction collection device. The unmetabolized parent fraction was calculated as the ratio of the sum of radioactivity in fractions containing the parent compound to the total amount of radioactivity collected. The fraction curve was also corrected by the time-varying extraction efficiency of radioactivity in corresponding filtered plasma sample. The arterial input function used for kinetic modeling was calculated as the product of the total plasma curve and the parent fraction curve.

The fraction of tracer unbound to plasma proteins was determined by ultrafiltration. Six mL of arterial blood taken immediate before radiotracer injection was spiked with approximately 370 kBq of [^{18}F]FP-(+)-DTBZ in a volume no greater than 0.2 mL. After 10 minutes incubation at room temperature, the spiked blood sample was centrifuged at 2300g for 5 minutes. Three replications of 0.2 mL of spiked plasma (supernatant) were counted with the automatic gamma counter. Spiked plasma 0.3 mL was loaded onto the reservoir of the Millipore Centrifree® micropartition devices in triplicate and centrifuged at 1100 g for 20 minutes. The pass-through unbound [^{18}F]FP-(+)-DTBZ was then collected and counted. The percentage of free fraction was calculated using the following equation: (radioactivity of unbound [^{18}F]FP-(+)-DTBZ)/(total radioactivity in plasma) × 100%.

Kinetic Modeling of PET Data

Summed radioactivity images were generated from each PET acquisition (session 1: 0 through 1.5–2 hours; session 2: 2.5 through 3.5–4 hours; session 3: 4.5 through 5.5–6 hours). Regions of interest (ROIs) for the pancreas (including head, body, and tail subregions) were manually delineated on the summed images from all acquisition sessions using the abdominal MRI to guide and confirm placement. ROIs for kidney were placed on the summed image from the first but not the second or third PET sessions because the renal cortex was not clearly discernible in the summed images from the later PET acquisitions. Radioactivity concentration in each ROI was extracted from the dynamic PET data to generate regional time-activity curves (TACs). High, sustained uptake of [^{18}F]FP-(+)-DTBZ was observed in the pancreas with concentration in head > tail ≥ body. Kinetics in renal cortex showed fast uptake with rapid washout. Compartment models using the arterial input function were applied to each TAC to estimate the total volume of distribution (V_T), an index of total tracer uptake relative to arterial plasma concentration (18). The complexity of the compartment model was determined by the quality of the model fits to the data. TACs from pancreas were modeled adequately by a model with one tissue compartment for 5 subjects; the remaining data sets were fitted well by a two-tissue model. Stable estimates of pancreatic V_T were typically achieved from 150 minutes of data, with shorter data sets generally yielding lower V_T values. Results from kinetic modeling of pancreas TACs reported in this manuscript are from 210–217 min of data with the exception of one control subject for whom only 160 min of data were acquired. TACs from kidney cortex were well-described by a two-tissue model. Estimates of renal VT obtained from the first scan session (from injection to 90–120 min) were reliable and used as an index of non-displaceable uptake (V_{ND}) for calculation of pancreatic binding potential (BP_{ND}), the equilibrium ratio of specific to non-displaceable tracer concentration (18), as has been done previously with [^{11}C]DTBZ (9).

Measurement of Radiometabolites in Pancreas of Nonhuman Primate

A [^{18}F]FP-(+)-DTBZ study was performed on a male rhesus macque (8.2yrs old; 8.78kg) in order to characterize the radioactivity in the pancreas with respect to the fractions of parent compound and radioactive metabolites. All study procedures were performed under a protocol approved by the Yale University Institutional Care and Use Committee. The animal

was sedated with an intramuscular injection of Ketamine hydrochloride and glycopyrrolate. The animal was transported to the PET facility and was intubated and maintained on oxygen and 2.0% isoflurane throughout the study. An i.v. was placed for the delivery of intravenous fluids and bolus injection of the tracer. A percutaneous arterial line was placed for the collection blood samples. A three minute bolus of 154 MBq [^{18}F]FP-(+)-DTBZ was given. Shortly before the end of the study, a blood sample was taken for plasma radioactivity analysis. While still under isoflurane anesthesia, the animal was euthanized 130 minutes post tracer injection with 3.0mL Euthasol via the saphenous vein. Death was verified by the cessation of heartbeat. The animal was transported to a procedure room for the collection of tissues. Four parts of pancreas tissue, including head, neck, body and tail, were first homogenized and denatured with equivalent volume of ethanol followed with a half amount of saline rinse, and then the mixtures were centrifuged for 10 min at 14,000 rpm to precipitate proteins. Activity in the supernatant from the pancreas tissue was monitored and up to 1.0 mL of sample was injected onto the reverse-phase HPLC analytical system with a retention time of the parent compound at 8 min. All the HPLC eluent was fraction-collected with an automated fraction collection device (CF-1 Fraction Collector, Spectrum Chromatography, Houston, TX, USA) in 2-min intervals and counted with the aforementioned automatic gamma counter. The counts of fractions were volume and decay corrected. [^{18}F]FP-(+)-DTBZ metabolite profile in plasma and pancreas was calculated as the ratio of the sum of radioactivity in the fraction containing the parent compound to the total amount of radioactivity collected.

Statistical Analysis

Quantitative results are presented as the mean value ± standard deviation unless otherwise noted. Differences between groups were analyzed using a two-tailed t-test with heteroscedastic variance. Relationships between mean pancreatic PET binding parameters and β-cell function as measured by the arginine stimulus test were assessed using the Pearson's correlation coefficient. All tests were performed using the GraphPad Prism 5 software. $P<0.05$ was considered statistically significant.

RESULTS

Measures of β-Cell Function

The time course and cumulative amounts of circulating C-peptide levels released following arginine administration are shown in Figure 1. Arginine stimulus induced significantly less C-peptide (0.117±0.161 vs. 6.25±1.72 pmol·mL^{-1}·min, $P<0.001$) in T1DM patients than controls, evidencing loss of β-cell function in the disease state.

In the subset of subjects who underwent hyperglycemic-glucagon stimulation tests (19,20), glucose levels were higher in the T1DM group in the first 30 minutes during the commencement of insulin infusion but were stable with no statistical difference between the groups for the last 45 minutes of the euglycemic and hyperglycemic phase of the clamp (Supplemental Figure 1A). The C-peptide responses in healthy volunteers gradually increased throughout the glucose clamp (Supplemental Figure 1B). The peak response was seen at 214 minutes (4 minutes after the glucagon bolus). The C-peptide response in subjects with type 1 diabetes was undetectable both during the clamp and following glucagon administration. These results confirm the absence of functional BCM in the T1DM subjects.

Arterial Blood Measurements

[^{18}F]FP-(+)-DTBZ showed a moderate rate of metabolism and clearance, with approximately 50% of the total plasma radioactivity attributable to radiometabolites at 30 minutes post-injection (Figure 2A). The plasma parent fraction did not differ significantly

between groups at any time after injection. Plasma free fraction had low intersubject variability (11.2% coefficient of variation) and did not differ between patient groups (22.4±3.0% in controls vs. 21.7±1.7% in T1DM, P=0.53; Figure 2B).

Analysis of PET Image Data

Qualitative assessment of PET images showed a striking difference between control and diabetic subjects in pancreatic [^{18}F]FP-(+)-DTBZ concentration, as seen in representative images shown in Figure 3 (images for all subjects are shown in Supplemental Figure 2 and rotating maximum intensity projections in Supplemental Videos 1–16). Concentration of radioactivity normalized by injected dose and body weight (standardized uptake value, or SUV) was significantly lower in pancreas of T1DM patients (n=7) than control subjects (n=9) by 37.7% (10.7±2.6 vs. 17.2±4.0, P=0.002) but did not differ in the kidney cortex (3.01±0.34 vs. 2.90±0.48, P=0.60) as shown in Figure 4A.

Regional V_T (reflecting total uptake of tracer relative to plasma) and pancreatic BP_{ND} (indicative of specific binding compared to a reference region having only non-displaceable uptake) are compared between groups (n=8 control, n=6 T1DM) in Figure 4B,C. Total tracer uptake per unit volume of whole pancreas was reduced by 19.8% in T1DM compared to controls at trend level significance (V_T equal 122±40 in T1DM vs. 152±42 in controls, P=0.14). V_T in renal cortex was slightly elevated in T1DM relative to controls but did not differ significantly between groups (P=0.29). A significant reduction of pancreatic specific binding density was observed in diabetic patients, with mean group difference of 40.0% (BP_{ND} equal 3.78±1.13 in T1DM vs. 6.30±1.75 in controls, P<0.01). It is improbable that these results reflect anything other than true tracer binding reductions in pancreas of T1DM patients because groups were well matched in all regards except disease state (Table 1). Binding estimates showed some association with patient age and body mass index (Supplemental Figure 3). The statistical significance of group differences in tracer binding remained intact when age and body mass index were included as covariates.

The PET binding parameters SUV, V_T and BP_{ND} are density metrics reflecting relative tracer concentrations per unit volume of tissue. In order to determine total tracer uptake in pancreas, we multiplied the PET outcome parameters by the whole pancreas volume measured from anatomical magnetic resonance images. Both absolute pancreas volume and pancreas volume normalized to body surface area (24) were significantly decreased in T1DM patients (Table 1). Scaling the binding parameters to account for pancreas volume enhanced the group differences in pancreatic uptake (Figure 4D–F). In particular, the 32% reduction in pancreas volume together with the 40% decrease in BP_{ND} gave a calculated 59% loss in total specific binding in the T1DM patients (207±91 cm^3 vs. 503±183 in controls, P<0.005; Figure 4F).

Relationship Between Radiotracer Binding and β-Cell Function

The tracer binding parameters SUV, V_T, and BP_{ND} were plotted against arginine-elicited C-peptide release to assess the relationship between [^{18}F]FP-(+)-DTBZ binding in pancreas and β-cell function (Figure 5A–C). The significant correlations of tracer binding parameters with C-peptide release suggest that not only does [^{18}F]FP-(+)-DTBZ PET discriminate between healthy controls and T1DMs, but that PET binding measures quantitatively reflect β-cell function. Interestingly, the control subject that exhibited much lower BP_{ND} than others in the group was also found to have a blunted response to arginine stimulus, further supporting the association between [^{18}F]FP-(+)-DTBZ binding and insulin-secretory capacity. Extrapolating the tracer binding measures to reflect total binding within the entire pancreas by accounting for pancreas volume strengthened the correlations of the PET binding parameters with C-peptide released in response to the arginine stimulus (Figure 5D–

F). If the relationship between tracer binding and β-cell function holds across populations (e.g., T2DM or recent-onset T1DM), [^{18}F]FP-(+)-DTBZ PET would be a valuable tool for prognostics, longitudinal studies in humans or preclinical animal models for the development of therapeutic strategies or treatment monitoring.

Radiometabolites in Pancreas of Nonhuman Primate

HPLC analysis of the radioactivity in pancreas from the nonhuman primate study revealed that 90–93% of total radioactivity in pancreas represented the unchanged [^{18}F]FP-(+)-DTBZ, with no noticeable difference among 4 parts (head, neck, body, and tail). In the plasma sample acquired shortly before the end of the study, only 8% of the radioactivity was attributable to parent compound. Those metabolites detected in pancreas appear to have similar retention time as parts of non-polar metabolites observed in the plasma. Thus, while there were significant radioactive metabolites in the plasma, these data suggest that uptake of radioactive metabolites into the pancreas in the nonhuman primate is minimal, which is an important assumption in the modeling methods used here.

DISCUSSION

[^{18}F]FP-(+)-DTBZ is a recently developed PET tracer that can be used for the quantitative measurement of endogenous pancreatic islet β-cell mass in humans. Pancreatic BP_{ND}, the tracer specific binding per unit volume of tissue, was reduced by 40% ($P<0.01$) in C-peptide negative T1DM patients compared to healthy individuals matched for age and body mass index. When atrophy of the T1DM pancreas was accounted for, we observed a 59% reduction in total [^{18}F]FP-(+)-DTBZ binding in the pancreas. Moreover, [^{18}F]FP-(+)-DTBZ binding potential correlated positively ($R^2=0.59$, $P=0.002$) with the insulin secretory capacity of β-cells as measured by an arginine challenge. This relationship was further enhanced by accounting for pancreas volume to obtain total BCM binding ($R^2=0.78$, $P<0.0001$). These results indicate that PET imaging of [^{18}F]FP-(+)-DTBZ provides quantitative measures of pancreatic BCM. This noninvasive method is poised for use in interventional studies to prevent or reverse diabetes.

PET imaging with [^{18}F]FP-(+)-DTBZ yields measurements of endogenous BCM, in contrast to alternative methods that detect exogenous β-cells labeled prior to islet graft transplantation (25,26). Although the imaging of endogenous and exogenous BCM may prove complementary in clinical islet transplantation, quantitative measurements of endogenous BCM such as those provided by [^{18}F]FP-(+)-DTBZ PET are necessary for the pursuit of other avenues in research and medical practice. The ability to non-invasively and quantitatively measure endogenous pancreatic islet β-cell mass is necessary to reach a clearer understanding of the pathophysiology of the islet β-cells prior to and following the onset of diabetes mellitus. In addition, non-invasive measurement of innate BCM holds promise as a useful tool to monitor and test the efficacy of newly developed therapeutic approaches targeting preservation or restoration of healthy β-cell function. An appropriate insulin secretory response is ultimately dependent upon β-cell capacity, which is determined by both the β-cell mass and its responsiveness to circulating metabolite and hormonal cues that stimulate insulin secretion. Current methods used to evaluate β-cell capacity are limited to those that measure insulin release in response to a mixed meal tolerance test, arginine or glucagon stimulation tests, or hyperglycemic clamps. All of these methodologies suffer from the uncertainty that the insulin secretory response can be modulated by factors such as recent glucose control, adolescence, adiposity, and insulin resistance. Consequently, these measures of β-cell function are unable to distinguish between a robust secretory response from a few islets versus a weaker response from a greater number of islets. An assessment of β-cell capacity that can distinguish between mass and function would aid the development

of treatments to enhance stimulated insulin secretion of patients with Type 1 or Type 2 diabetes.

The validity of VMAT2 as a target for β-cell imaging has been a topic of lively debate (27,28). *In vitro* experiments have yielded discrepant results, with some studies finding that VMAT2 density was highly co-localized with insulin expression (14–16), while others reported that total binding signal of VMAT2 ligands reflected mechanisms independent of BCM (29). Yet other histological studies revealed that VMAT2 is expressed in pancreatic polypeptide cells outside of islet β-cells and that [^{18}F]FP-(+)-DTBZ binds saturably at a low-affinity non-VMAT2 site; however, VMAT2 expression and [^{18}F]FP-(+)-DTBZ binding were still strongly correlated with β-cell density despite the contribution of background signal from off-target sites (30,31). Indeed, our own work using [^{11}C]DTBZ and [^{18}F]FP-(+)-DTBZ for *in vivo* imaging in rats found a significant correlation between VMAT2 binding and insulin expression even though a substantial specific binding signal remained after elimination of β-cells by streptozotocin administration.[17] These findings are consistent with the present study in which we found significant quantitative relationships between [^{18}F]FP-(+)-DTBZ binding and insulin secretory capacity despite the fact that T1DM patients exhibited residual pancreatic binding, which could be attributable to tracer binding at non-β-cell sites or residual β-cell mass (32). Although we cannot distinguish background binding due to a non-VMAT2 binding site distinct from the presence of VMAT2 outside β-cells, changes in non-specific binding can be corrected by the use of an appropriate reference region. Studies in rats using [^{18}F]FP-(+)-DTBZ blocked by the unlabeled compound and preliminary experiments in baboon using [^{18}F]FP-(+)-DTBZ and its inactive enantiomer [^{18}F]FP-(−)-DTBZ demonstrated that the kidney cortex is an appropriate reference tissue for measuring specific binding in pancreas (17,33). In this study we found no significant group differences in renal SUV or V_T and used this region to calculate our specific binding outcomes, as has been done previously with [^{11}C]DTBZ (9). The spleen has been suggested as an alternative reference tissue and when applied as such yielded overall outcome trends very similar to the kidney, but with reduced BP_{ND} estimates and increased variability. Although preliminary data in baboon show it to be a non-ideal reference tissue (33), the spleen should be insensitive to diabetes-induced renal failure and if further validated might serve as an imperfect but practical reference region in clinical populations.

A potential limitation of imaging the pancreas with PET is the concept of partial volume effect that may lead to an underestimation of the radioactivity concentration measured in a small structure such as an individual islet or lung nodule (34). The PET signal measured in any given location is influenced by the spatial resolution of the scanner compared to the size of the object being imaged, as well as the contrast of concentration in the tissue relative to its surroundings. The partial volume effect describes the underestimation of radioactivity concentration in hot spots that suffer from “spill-out” of signal, and overestimation in low activity regions that are contaminated by “spill-in” from adjacent high activity objects. However, as discussed by Ichise and Harris (28), PET imaging of BCM is conceptually distinct from that of diagnostic imaging of lung nodules where partial volume effects are important. The correction for partial volume effects is needed for quantifying the tracer concentration in individual lung nodules where the goal is to distinguish between benign and malignant tumors. In contrast, the goal of quantifying BCM is not to determine the uptake within individual islets, but to measure an integrated signal of [^{18}F]FP-(+)-DTBZ within the pancreas. These studies are exactly analogous to the use of PET tracers for quantitative imaging of neuroreceptors, where corrections for partial volume effects are not necessary to determine the density of target sites in a given volume of tissue.

Nevertheless, our analysis methods were designed to minimize any potential partial volume effects in the measurement of radioactivity concentration in the pancreas. The pancreas tends to be smaller in T1DM patients than controls, a finding reported previously (24,35) and replicated in our magnetic resonance imaging studies (Table 1). This atrophy could potentially lead to underestimation of pancreatic PET signal in T1DM. As a precautionary measure, regions of interest (ROIs) were drawn conservatively along the central axis of the pancreas to exclude voxels at the edge of the organ susceptible to signal spill-out. The cross-sectional width of pancreas ROIs rarely exceeded 2 voxels (5.1 mm) in the body and tail or 3 voxels (7.7 mm) in the head of the organ. Previous ultrasound (36) and computed tomography (37) imaging studies reported typical pancreas diameters of 12–20 mm in the head and 9–14 mm in body and tail of T1DM patients with slightly greater values in control subjects. Respiratory motion further increases the effective size of the pancreas in our PET images. By comparison, the spatial resolution of reconstructed images from the HR+ PET camera is approximately 6 mm (22). Given the spatial resolution of the scanner, the effective size of the pancreas, and our intentional omission of pancreas voxels susceptible to signal spill-out, any errors introduced by partial volume effects should be minor. Hence it is highly unlikely that the group differences observed in [^{18}F]FP-(+)-DTBZ binding are attributable to bias induced by partial volume effects.

CONCLUSION

The results reported here indicate that PET imaging of [^{18}F]FP-(+)-DTBZ can non-invasively and quantitatively measure clinically relevant changes in pancreatic BCM. We validated [^{18}F]FP-(+)-DTBZ PET through quantitative imaging using kinetic modeling with arterial input functions and found markedly reduced [^{18}F]FP-(+)-DTBZ binding density in patients with long-standing T1DM compared to well-matched healthy controls. In comparison to [^{11}C]DTBZ, [^{18}F]FP-(+)-DTBZ had substantially improved dynamic range of pancreatic binding parameters correlating with β-cell function, such that the functional loss of β-cell density in T1DM was discernible without depending on anatomical differences in pancreas volume. Accounting for pancreas volume, to obtain parameters indicative of total pancreatic binding, enhanced group differences in tracer binding and improved the quantitative relationship between the PET outcomes and insulin secretion capacity. These studies suggest that PET imaging with [^{18}F]FP-(+)-DTBZ can be employed to quantify BCM, and β-cell capacity when combined with assays of β-cell function. The present work and previous studies indicate that the kidney cortex is an appropriate reference tissue that lacks specific binding and exhibits small inter-subject variability (9,17,33). The existence of such a reference region may obviate the need for arterial blood sampling, thereby simplifying data analysis and reducing the cost, complexity, and invasiveness of the imaging procedure. Finally, we note that the longer radioactive half-life of ^{18}F (109.8 minutes) as compared to ^{11}C (20.4 minutes) facilitates distribution of [^{18}F]FP-(+)-DTBZ over wide geographic regions, as is currently done with [^{18}F]fluorodeoxyglucose ([^{18}F]FDG). The feasibility of centralized production will minimize costs and enable research trials or clinical applications at imaging centers that lack the radiochemistry infrastructure or expertise necessary to synthesize [^{18}F]FP-(+)-DTBZ on-site.

Supplementary Material

Refer to Web version on PubMed Central for supplementary material.

Acknowledgments

This work was funded by the Yale-Pfizer Bioimaging Research Alliance, NIH UL1 RR024139, and NIH R01 AG-23686. Expert technical assistance was provided by the staff of Avid Radiopharmaceuticals, the Yale PET

Center, Yale Magnetic Resonance Research Center, and the Yale Center for Clinical Investigation. KFP is the recipient of a Distinguished Clinical Scientist Award from the American Diabetes Association. MDN acknowledges the support of NIH T32 DA022975.

Financial support: This work was funded by the Yale-Pfizer Bioimaging Research Alliance, NIH UL1 RR024139, and NIH R01 AG-23686.

REFERENCES

1. Schmitz A, Shiue CY, Feng Q, et al. Synthesis and evaluation of fluorine-18 labeled glyburide analogs as beta-cell imaging agents. Nucl Med Biol. 2004; 31:483–491. [PubMed: 15093819]
2. Schneider S, Feilen PJ, Schreckenberger M, et al. In vitro and in vivo evaluation of novel glibenclamide derivatives as imaging agents for the non-invasive assessment of the pancreatic islet cell mass in animals and humans. Exp Clin Endocrinol Diabetes. 2005; 113:388–395. [PubMed: 16025400]
3. Wangler B, Beck C, Shiue CY, et al. Synthesis and in vitro evaluation of (S)-2-([11 C]methoxy)-4-[3-methyl-1 -(2-piperidine-1 -yl-phenyl)-butyl-carbamoyl]-benzoic acid ([11C]methoxy-repaglinide): a potential beta-cell imaging agent. Bioorg Med Chem Lett. 2004; 14:5205–5209. [PubMed: 15380228]
4. Garcia A, Mirbolooki MR, Constantinescu C, et al. 18F-Fallypride PET of pancreatic islets: in vitro and in vivo rodent studies. J Nucl Med. 2011; 52:1125–1132. [PubMed: 21680697]
5. Kung HF, Lieberman BP, Zhuang Z-P, et al. In vivo imaging of vesicular monoamine transporter 2 in pancreas using an 18F epoxide derivative of tetrabenazine. Nucl Med Biol. 2008; 35:825–837. [PubMed: 19026944]
6. Kung M-P, Hou C, Lieberman BP, et al. In vivo imaging of β-cell mass in rats using 18F-FP-(+)-DTBZ: A potential PET ligand for studying diabetes mellitus. J Nucl Med. 2008; 49:1171–1176. [PubMed: 18552132]
7. Simpson NR, Souza F, Witkowski P, et al. Visualizing pancreatic β-cell mass with [11C]DTBZ. Nucl Med Biol. 2006; 33:855–864. [PubMed: 17045165]
8. Souza F, Simpson N, Raffo A, et al. Longitudinal noninvasive PET-based β-cell mass estimates in a spontaneous diabetes rat model. J Clin Invest. 2006; 116:1506–1513. [PubMed: 16710474]
9. Goland R, Freeby M, Parsey R, et al. 11C-Dihydrotetrabenazine PET of the pancreas in subjects with long-standing type 1 diabetes and in healthy controls. J Nucl Med. 2009; 50:382–389. [PubMed: 19223416]
10. Weihe E, Schafer MK, Erickson JD, Eiden LE. Localization of vesicular monoamine transporter isoforms (VMAT1 and VMAT2) to endocrine cells and neurons in rat. J Molec Neurosci. 1994; 5:149–164. [PubMed: 7654518]
11. Weihe E, Eiden LE. Chemical neuroanatomy of the vesicular amine transporters. FASEB J. 2000; 14:2435–2449. [PubMed: 11099461]
12. Bohnen NI, Albin RL, Koeppe RA, et al. Positron emission tomography of monoaminergic vesicular binding in aging and Parkinson disease. J. Cereb Blood Flow Metab. 2006; 26:1198–1212. [PubMed: 16421508]
13. Martin WR, Wieler M, Stoessl AJ, Schulzer M. Dihydrotetrabenazine positron emission tomography imaging in early, untreated Parkinson(s disease. Ann Neurol. 2008; 63:388–394. [PubMed: 18240153]
14. Anlauf MR, Eissele MK, Schafer LE, et al. Expression of the two isoforms of the vesicular monoamine transporter (VMAT1 and VMAT2) in the endocrine pancreas and pancreatic endocrine tumors. J Histochem Cytochem. 2003; 51:1027–1040. [PubMed: 12871984]
15. Maffei AZ, Liu P, Witkowski F, et al. Identification of tissue-restricted transcripts in human islets. Endocrinology. 2004; 145:4513–4521. [PubMed: 15231694]
16. Harris PE, Ferrara C, Barba P, Polito T, Freeby M, Maffei A. VMAT2 gene expression and function as it applies to imaging beta-cell mass. J Molec Med. 2008; 86:5–16. [PubMed: 17665159]

17. Singhal T, Ding Y-S, Weinzimmer D, et al. Pancreatic beta cell mass PET imaging and quantification with [11C]DTBZ and [18F]FP-(+)-DTBZ in rodent models of diabetes. Mol Imag Biol. 2011; 13:973–984.
18. Innis RB, Cunningham VJ, Delforge J, et al. Consensus nomenclature for in vivo imaging of reversibly binding radioligands. J Cereb Blood Flow Metab. 2007; 27:1533–1539. [PubMed: 17519979]
19. Keymeulen B, Vandemeulebroucke E, Ziegler AG, et al. Insulin needs after CD3-antibody therapy in new-onset type 1 diabetes. N Engl J Med. 2005; 352:2598–2608. [PubMed: 15972866]
20. DeFronzo RA, Tobin JD, Andres R. Glucose clamp technique: a method for quantifying insulin secretion and resistance. Am J Physiol. 1979; 237:E214–E223. [PubMed: 382871]
21. Papademetris, X.; Jackowski, M.; Rajeevan, N.; Constable, RT.; Stain, LH. BioImage Suite: An integrated medical image analysis suite. http://www.bioimagesuite.org
22. Brix G, Zaers J, Adam LE, et al. Performance evaluation of a whole-body PET scanner using the NEMA protocol. J Nucl Med. 1997; 38:1614–1623. [PubMed: 9379202]
23. Hilton J, Yokoi F, Dannals RF, Hayden TR, Szabo Z, Wong DF. Column-switching HPLC for the analysis of plasma in PET imaging studies. Nucl Med Biol. 2000; 27:627–630. [PubMed: 11056380]
24. Goda K, Sasaki E, Nagata K, Fukai M, Ohsawa N, Hahafusa T. Pancreatic volume in type 1 and type 2 diabetes mellitus. Acta Diabetol. 2001; 38:145–149. [PubMed: 11827436]
25. Evgenov NV, Medarova Z, Dai G, Bonner-Weir S, Moore A. In vivo imaging of islet transplantation. Nat Med. 2006; 12:144–148. [PubMed: 16380717]
26. Kim S-J, Doudet DJ, Studnov AR, Nian C, Ruth TJ, Gambhir SS. Quantitative micro positron emission tomography (PET) imaging for the in vivo determination of pancreatic islet graft survival. Nat Med. 2006; 12:1423–1428. [PubMed: 17143277]
27. Kwee TC, Basu S, Saboury B, Torigian DA, Naji A, Alavi A. Beta-cell imaging: opportunities and limitations. J Nucl Med. 2011; 52:493. [PubMed: 21321278]
28. Ichise M, Harris PE. Reply: Beta-cell imaging: opportunities and limitations. J Nucl Med. 2011; 52:493–495. [PubMed: 21321278]
29. Fagerholm V, Mikkola KK, Ishizu T, et al. Assessment of islet specificity of dihydrotetrabenazine radiotracer binding in rat pancreas and human pancreas. J Nucl Med. 2010; 51:1439–1446. [PubMed: 20720057]
30. Saisho Y, Harris PE, Butler AE, et al. Relationship between pancreatic vesicular monoamine transporter 2 (VMAT2) and insulin expression in human pancreas. J Mol Hist. 2008; 39:543–551.
31. Tsao H-H, Lin K-J, Juang J-H, et al. Binding characteristics of 9-fluoropropyl-(+)-dihydrotetrabenazine (AV-133) to the vesicular monoamine transporter type 2 in rats. Nucl Med Biol. 2010; 37:413–419. [PubMed: 20447551]
32. Keenan HA, Sun JK, Levine J, et al. Residual insulin production and pancreatic β-cell turnover After 50 years of diabetes: Joslin Medalist study. Diabetes. 2010; 59:2846–2853. [PubMed: 20699420]
33. Ichise M, Slifstein M, Easwaramoorthy B, et al. VMAT2 imaging of baboons with two 18F-FP-DTBZ enantiomers [abstract]. J Nucl Med. 2009; 50:227.
34. Hickeson M, Yun M, Matthies A, et al. Use of corrected standardized uptake value based on the lesion size on CT permits accurate characterization of lung nodules on FDG-PET. Eur J Nucl Med. 2002; 29:1639–1647.
35. Williams AJK, Chau W, Callaway MP, Dayan CM. Magnetic resonance imaging: a reliable method for measuring pancreatic volume in type 1 diabetes. Diabet Med. 2007; 24:35–40. [PubMed: 17227322]
36. Silva ME, Vezzozo DP, Ursich MJ, Rocha DM, Cerri GG, Wajchenberg BL. Ultrasonographic abnormalities of the pancreas in IDDM and NIDDM patients. Diabetes Care. 1993; 16:1296–1297. [PubMed: 8404436]
37. Gilbeau J-P, Poncelet V, Libon E, Derue G, Heller FR. The density, contour, and thickness of the pancreas in diabetics: CT findings in 57 patients. AJR Am J Roentgenol. 1992; 159:527–531. [PubMed: 1503017]

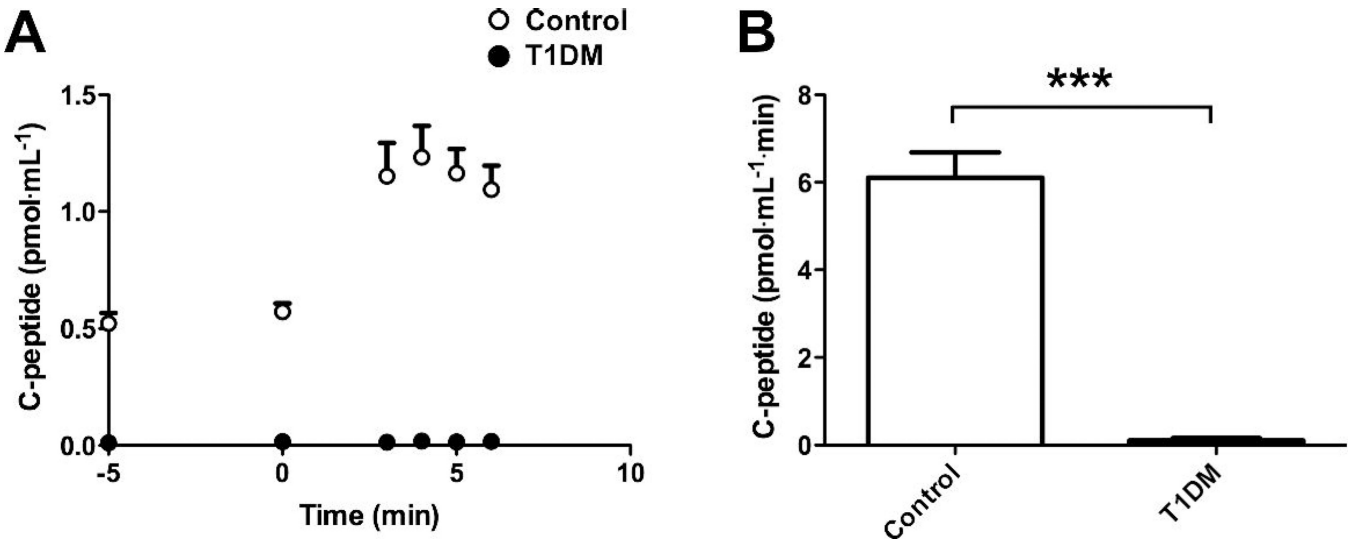

Figure 1.

C-peptide release as an indicator of β-cell function assessed by arginine stimulus test. (A) Circulating levels of C-peptide released in response to arginine administration were greater in control subjects (n=8) than diabetic patients (n=7), as were the areas under the curve (B). Data are expressed as mean ± s.e.m. Data from T1DM patients indicated by filled markers, control subjects by open markers. Error bars represent s.e.m. ** P<0.01, *** P<0.005.

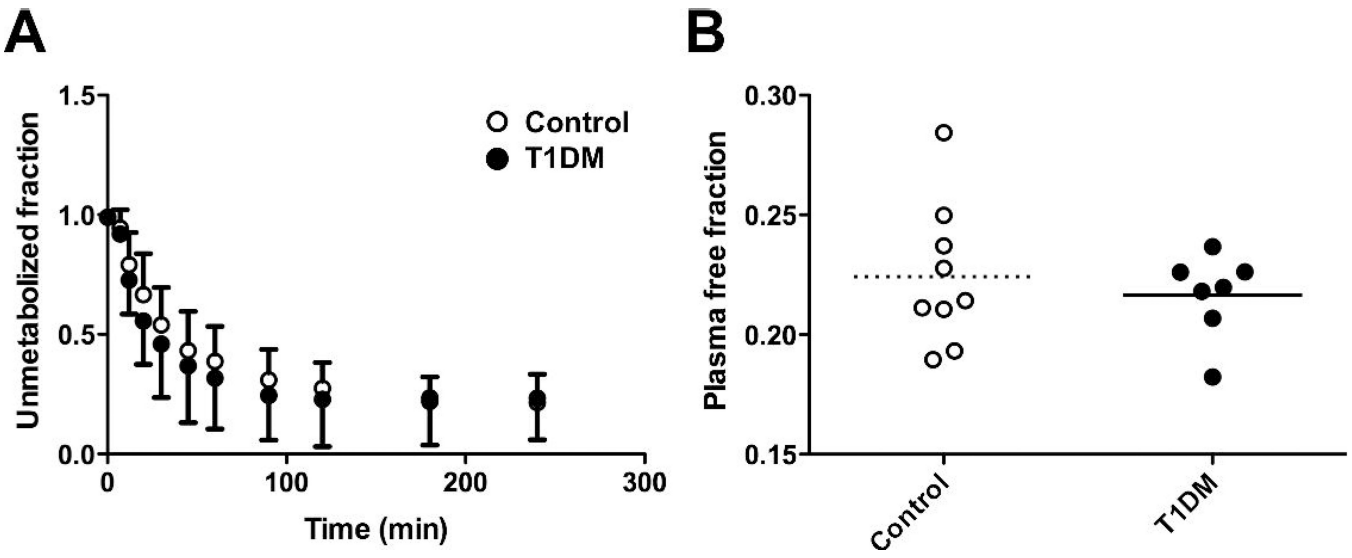

Figure 2.

Characteristics of [^{18}F]FP-(+)-DTBZ metabolism and availability in arterial blood. (A) The fraction of radioactivity in plasma attributable to the parent compound was not statistically different between groups ($0.23 < P < 0.94$ for *t* tests at each individual time point; $P=0.36$ for two-way ANOVA across time points common to all subjects). Data are expressed as mean ± s.d. (B) Fraction of radiotracer unbound to plasma proteins did not differ between groups (0.224±0.030 vs. 0.217±0.018, $P=0.53$). Horizontal lines represent mean for the respective cohort. Open markers: control subjects. Filled markers: T1DM patients.

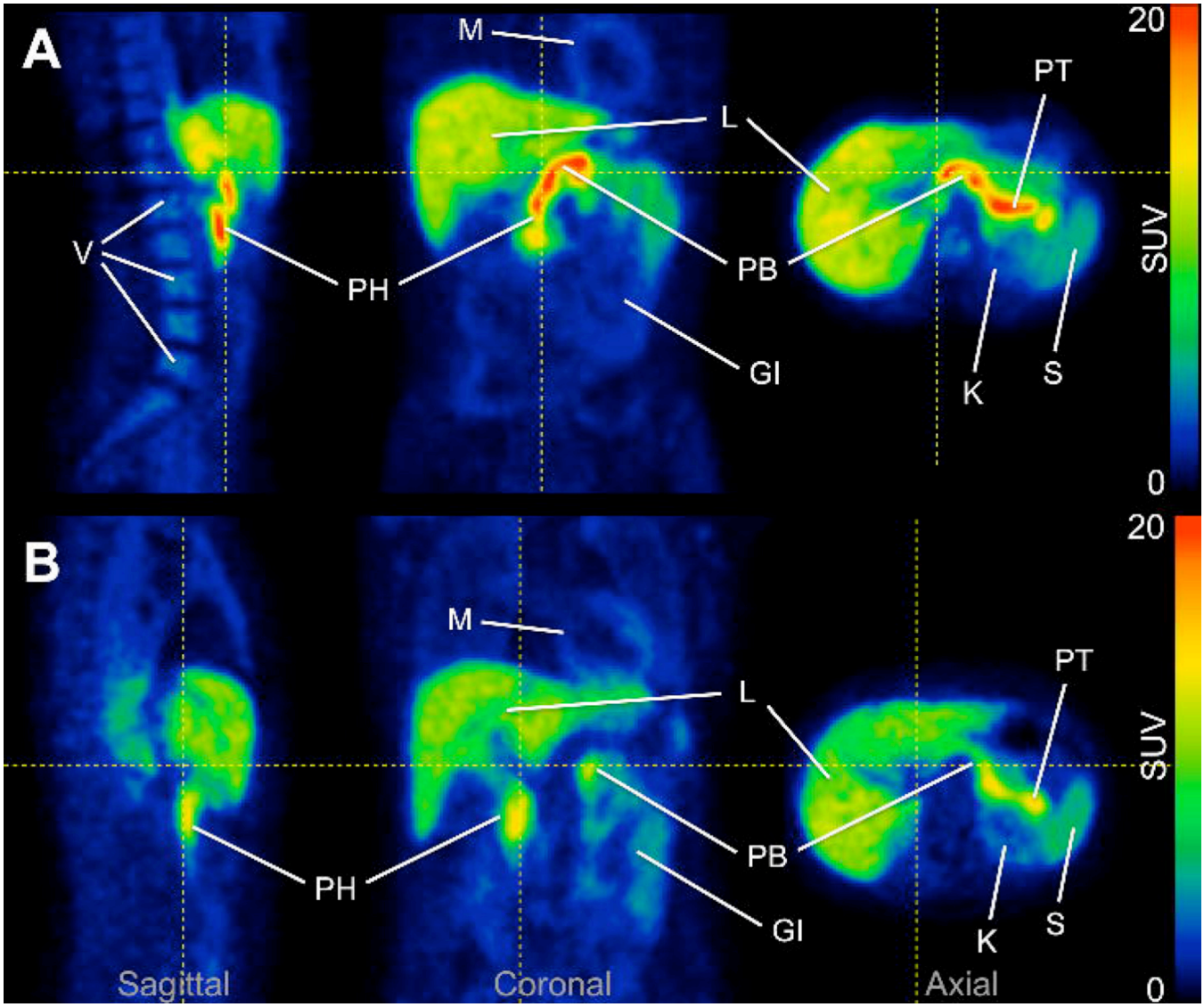

Figure 3.

Representative [^{18}F]FP-(+)-DTBZ PET images. (A) Image acquired in a healthy control subject showed high uptake of tracer in pancreas. (B) Pancreas uptake was reduced in a type 1 diabetes patient. Both images represent PET data summed from 0 to 90 min post-injection and are displayed on a common scale (0 to 20 SUV, i.e., radioactivity normalized by injected dose and body weight). PT: pancreas tail, PB: pancreas body, PH: pancreas head, L: liver, K: kidney, S: spleen, M: myocardium, V: vertebrae, GI: gastrointestinal tract. Images for entire cohort are displayed in Supplemental Figure 2. Maximum intensity projection animations are shown in the Supplemental Videos 1–16.

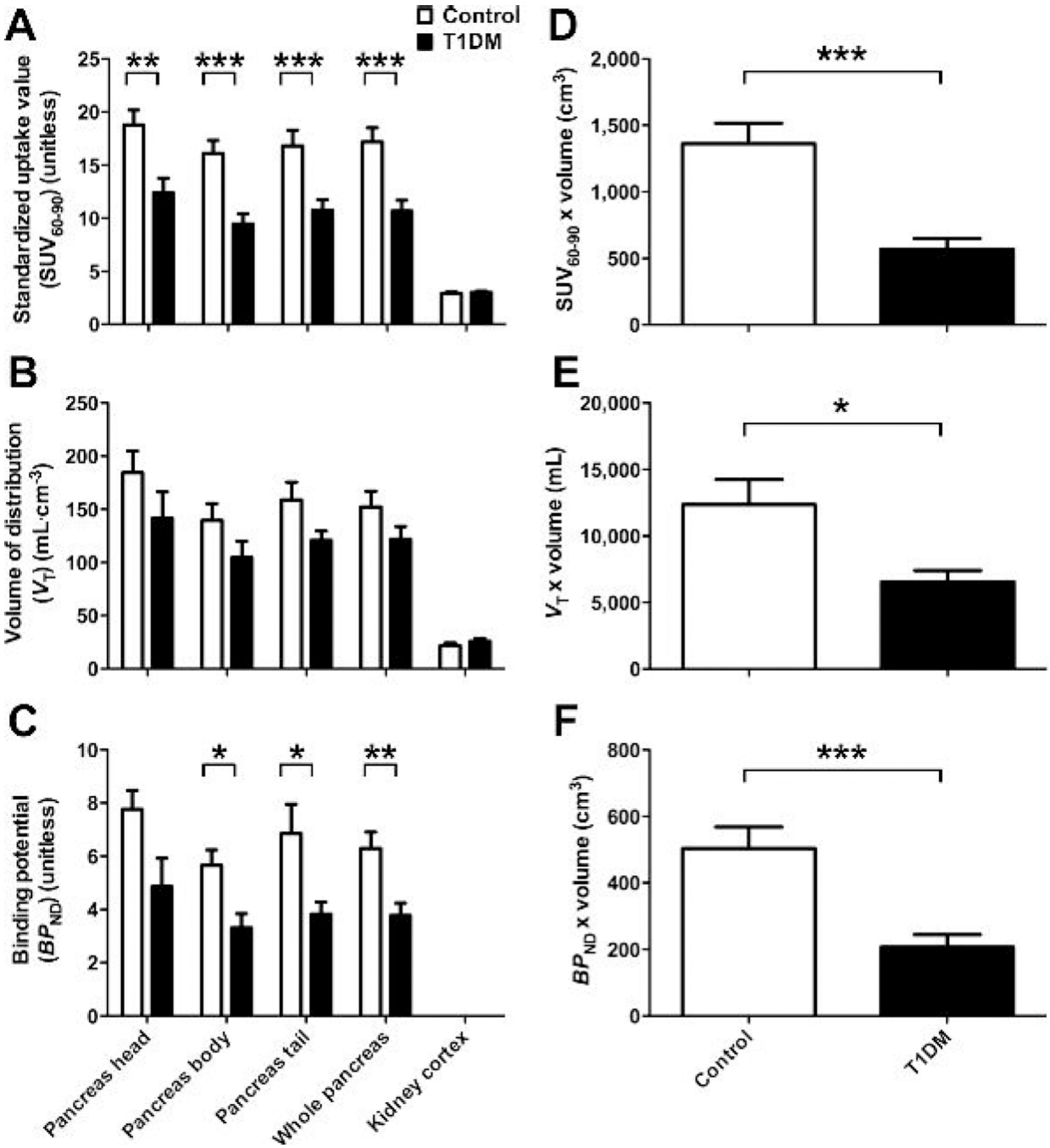

Figure 4.

[^{18}F]FP-(+)-DTBZ binding was reduced in T1DM patients vs. healthy control subjects. (A) Standardized uptake value (SUV^{60}–90 the concentration of tracer from 60–90 minutes normalized by injected dose and body weight, was significantly lower by 38% in pancreas of T1DM patients (n=7) as compared to controls (n=9). No significant difference in kidney SUV^{60}–90 was observed. (B) Volume of distribution *(V_T)*, which reflects the total uptake and retention of tracer relative to arterial plasma, was estimated in subjects for whom arterial blood was measured (n=8 control, n=6 T1DM). V_T was reduced by 20% in the pancreas of T1DM subjects at trend level significance. V_T in kidney cortex did not differ between groups. (C) Binding potential *(BP_{ND})*, which reflects tracer specific binding using kidney

V_T as an estimate of non-displaceable uptake, was significantly lower by 40% in the pancreas of T1 DM patients than healthy subjects. (D–F) Group differences in PET binding parameters estimated from whole pancreas are accentuated after correction for pancreas volume, which provides a measure of total tracer binding reflecting aggregate β-cell mass. Control subjects are designated by open bars, T1DM patients by filled bars. Data are expressed as mean ± s.e.m. * $P<0.05$, ** $P<0.01$, *** $P<0.005$.

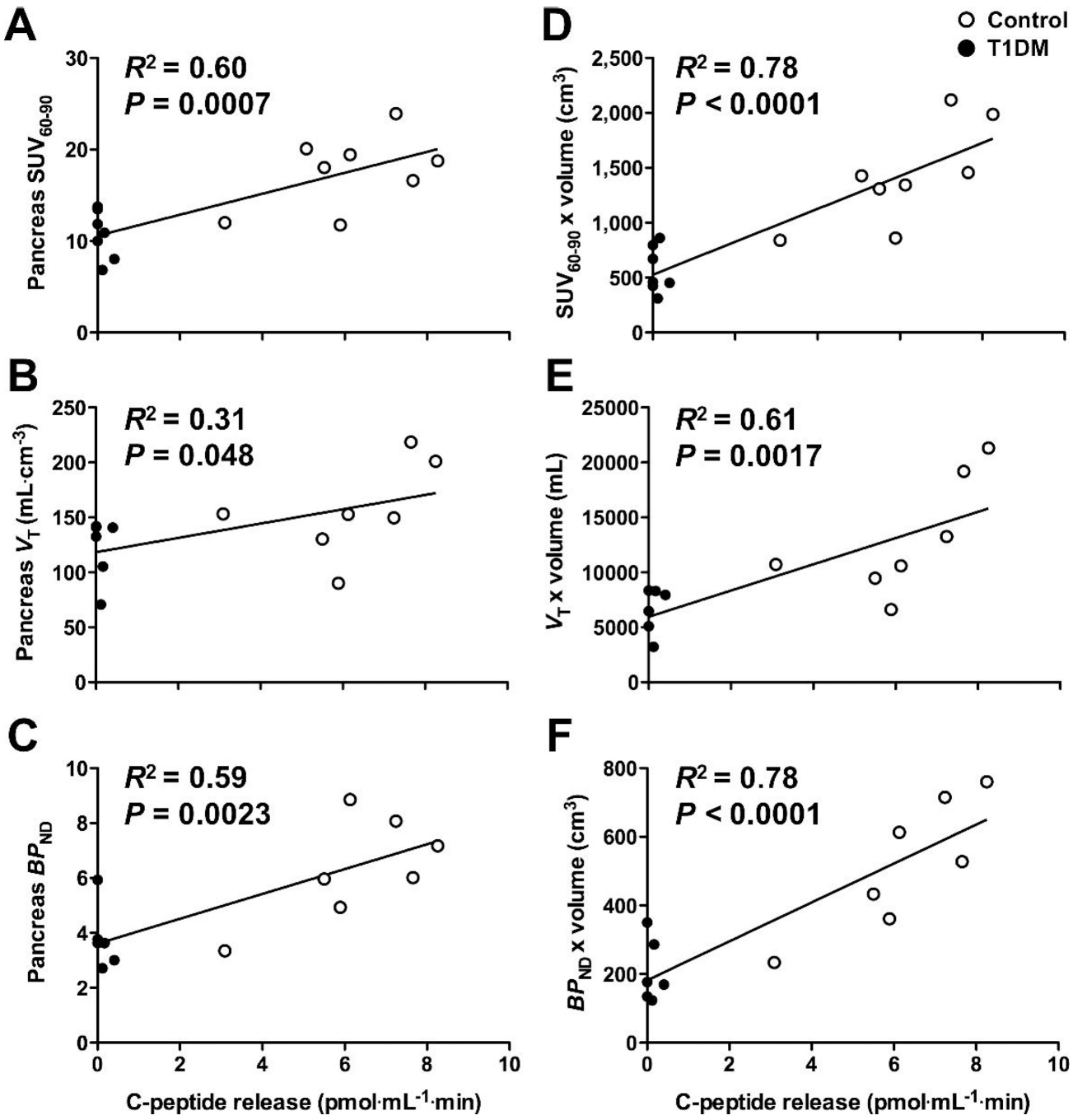

Figure 5.

Tracer binding density was associated with insulin secretory capacity. The pancreatic [^{18}F]FP-(+)-DTBZ uptake and binding density parameters SUV (A), V_T (B) and BP_{ND} (C) correlated positively with arginine-stimulated increases in circulating C-peptide, a metric of β-cell function. Multiplying [^{18}F]FP-(+)-DTBZ binding density parameters by pancreas volume to reflect total pancreatic binding improved their quantitative relationships with insulin secretory capacity (D–F). Data from T1DM patients indicated by filled markers, control subjects by open markers.

Table 1

Demographic and Laboratory Data

Parameter	Controls (*n*=9)	Patients (*n*=7)	*P*
Age (y)	34.2 ± 11.2	40.1 ± 8.6	0.271
Sex (male:female)	4:5	3:4	
BMI ($kg \cdot m^{-2}$)	24.6 ± 2.6	23.1 ± 2.9	0.153
Weight (kg)	71.6 ± 12.9	69.8 ± 10.9	0.769
Hemoglobin A1c (%)	5.4 ± 0.3	7.6 ± 2.1	0.019
Insulin dose per day ($units \cdot kg^{-1} \cdot d^{-1}$)	N/A	34.6 ± 14.2	NA
Duration of type 1 diabetes (y)	N/A	19.3 ± 13.9	NA
Estimated glomerular filtration rate	83.5 ± 8.7	94.7 ± 17.5	0.122
Pancreas volume (cm^3)	78.1 ± 13.3	52.9 ± 13.8	0.002
Pancreas volume index ($cm^3 \cdot m^{-2}$) (24)	43.0 ± 7.3	28.8 ± 6.2	0.001

Mean ± s.d., N/A = not applicable